Reovirus core proteins λ1 and σ2 promote stability of disassembly intermediates and influence early replication events

Stephanie Gummersheimer[a] and Pranav Danthi[ab]

[a]Department of Biology, Indiana University, Bloomington, Indiana, USA

Running Title: Reovirus core proteins influence entry and replication

[b]Corresponding author: Mailing address: Department of Biology, Indiana University 212 S. Hawthorne Drive, Bloomington IN 47405. Phone: (812) 856-2449 Fax: (812) 856-5710. E-mail: pdanthi@indiana.edu

ABSTRACT

The capsids of mammalian reovirus contain two concentric protein shells, the core and the outer capsid. The outer capsid is comprised of μ1-σ3 heterohexamers which surround the core. The core is comprised of λ1 decamers held in place by σ2. After entry into the endosome, σ3 is proteolytically degraded and μ1 is cleaved and exposed to form ISVPs. ISVPs undergo further conformational changes to form ISVP*s, resulting in the release of μ1 peptides which facilitate the penetration of the endosomal membrane to release transcriptionally active core particles into the cytoplasm. Previous work has identified regions or specific residues within reovirus outer capsid that impact the efficiency of cell entry. We examined the functions of the core proteins λ1 and σ2. We generated a reovirus T3D reassortant that carries strain T1L derived σ2 and λ1 proteins (T3D/T1L L3S2). This virus displays a lower ISVP stability and therefore converts to ISVP*s more readily. To identify the basis for lability of T3D/T1L L3S2, we screened for hyper-stable mutants of T3D/T1L L3S2 and identified three point mutations in μ1 that stabilize ISVPs. Two of these mutations are located in the C-terminal ϕ region of μ1, which has not previously been implicated in controlling ISVP stability. Independent from compromised ISVP stability, we also found that T3D/T1L L3S2 launches replication more efficiently and produces higher yields in infected cells. In addition to identifying a new role for the core proteins in disassembly events, these data highlight that core proteins may influence multiple stages of infection.

IMPORTANCE

Protein shells of viruses (capsids) have evolved to undergo specific changes to ensure the timely delivery of genetic material to host cells. The 2-layer capsid of reovirus

provides a model system to study the interactions between capsid proteins and the changes they undergo during entry. We tested a virus in which the core proteins were derived from a different strain than the outer capsid. We found that this mismatched virus was less stable and completed conformational changes required for entry prematurely. Capsid stability was restored by introduction of specific changes to the outer capsid, indicating that an optimal fit between inner and outer shells maintains capsid function. Separate from this property, mismatch between these protein layers also impacted the capacity of virus to initiate infection and produce progeny. This study reveals new insights into the roles of capsid proteins and their multiple functions during viral replication.

INTRODUCTION

In order to successfully launch replication, a virus must protect, transport and deliver its genome into the host cell. The viral capsid is a complex mechanical container with the primary function of assembling around the viral genome in one host cell, exiting that host cell and releasing the genome in another host cell. Therefore, the capsid has two demands that appear to be in direct conflict with one another. It must be stable enough to protect and transport the viral genome, but it also must be dynamic, poised to react to the right environment at the right time to perform functions during entry and to allow for replication of the genome. Viruses have evolved capsid proteins that are capable of these dynamic mechanical interactions in a number of diverse and fascinating ways. While some capsids are made up of only a single type of capsid protein, others have more complex combinations of proteins. One family of viruses, *Reoviridae*, have double or even triple layered capsids.

The *Reoviridae* family of viruses is made up of non-enveloped virions with capsids that are composed of 1 to 3 concentric protein shells that surround 9 to 12 ds RNA genome segments (1–3). While the outer layers of the multilayered capsids are proteolytically processed and undergo conformational changes during entry, the innermost capsid or core which contains the genome, remains intact throughout the remainder of replication (4). The core is a complex molecular machine that is capable of producing fully capped and functional RNA transcripts for translation by the host machinery (5, 6). The capsid proteins must, therefore, be capable of multiple functions in addition to their protective and structural roles. The outer capsid proteins must be poised to undergo the conformational changes required to release the cores and allow

78 them to be transcriptionally active. While studies of mammalian reovirus have provided
79 many insights into how outer capsid proteins regulate and mediate entry events that
80 lead to these conformational changes, the role of the core proteins in cell entry events
81 remains unclear.

82 The capsids of mammalian reovirus are made up of two concentric protein shells,
83 the core and the outer capsid (4). The outer capsid is primarily made up of μ1-σ3
84 heterohexamers (7) (Fig 1). These surround the core which is comprised of λ1
85 decamers held in place by σ2 (8). Turrets, made up of λ2 pentamers, protrude from the
86 core at the five-fold axis of symmetry. The σ1 attachment protein forms trimers that are
87 anchored in the λ2 turret (8, 9). After entry, σ3 is proteolytically degraded within the
88 endosome and μ1 is cleaved into μ1δ and μ1ϕ fragments (10, 11). These μ1 fragments
89 remain particle associated at this stage and the particle is referred to as an infectious
90 subvirion particle or ISVP (12–14). Further conformational changes within the
91 endosome result in cleavage of μ1δ to form μ1N and δ (15, 16). These particles are no
92 longer infectious and are referred to as ISVP*. Release of μ1 peptides (μ1N and ϕ)
93 results in penetration of the endosomal membrane and the deposition of the
94 transcriptionally active cores into the cytoplasm (13, 17, 18).

95 Previous work in identifying interactions and proteins involved in reovirus
96 disassembly and cell entry have focused on the outer capsid proteins. Here, we focused
97 on the structural functions of the core proteins λ1 and σ2. We characterized a
98 reassortant virus containing the λ1 encoding gene segment L3 and the σ2 encoding
99 gene segment S2 (T3D/T1L L3S2). We found that this new virus displays a higher
100 ISVP-to-ISVP* conversion efficiency or lower ISVP stability. We identified three point

mutations in μ1 that increase the stability of T3D/T1L L3S2. Two of these mutations are located in the ϕ region of μ1, which has not previously been implicated in maintaining ISVP stability or controlling ISVP-to-ISVP* conversion. Additionally, this reassortant virus has increased growth resulting from higher transcription levels and, subsequently, higher protein production. This role does not appear to be related to the enhanced ISVP-to-ISVP* conversion of this virus. These results provide insights into understanding the structural functions of the core proteins and how their interactions may influence disassembly and early replication steps during infection.

RESULTS

ISVP to ISVP* conversion efficiency of T3D is altered by the T1L core proteins λ1 and σ2. Single gene reassortants between prototype reovirus strains T1L and T3D, which contain mismatches between outer capsid proteins, display altered capsid stability and efficiency of disassembly intermediate formation (19–21). To determine whether the core proteins λ1 and σ2 play a role in ISVP-to-ISVP* conversion efficiency, we characterized the properties of T3D/T1L L3S2. This virus contains the λ1-encoding gene segment L3 and the σ2-encoding gene segment S2 from T1L in an otherwise T3D genetic background. The resulting virus therefore contains major core proteins that do not match the outer capsid. The λ1 protein from T3D and T1L are 99.3% identical (9 amino acid differences out of 1,275) and the σ2 proteins are 98.8% identical (5 amino acid differences out of 418) (22–24). While σ2 interacts with the outer capsid μ1 trimer, λ1 is not known to interact with any outer capsid proteins (25).

To test overall virion stability, we incubated T3D and T3D/T1L L3S2 over a series of elevated temperatures and tested the protease stability of the major viral capsid proteins. Such an approach has been used previously to test stability of virions and viral entry intermediates (19). Based on the similarity in their protease sensitivity profiles, we think that virions of T3D/T1L L3S2 do not display significant changes in stability in comparison to the parent strain, T3D (Fig 2A). To determine if the mismatches in this reassortant virus alter stability of ISVPs or efficiency of ISVP-to-ISVP* conversion, we generated ISVPs of T3D and T3D/T1L L3S2 and incubated them over a gradient of increasing temperatures. ISVP* conversion was determined as a measure of trypsin sensitivity of the μ1 δ fragment (26). In comparison to the parent strain T3D, T3D/T1L L3 ISVPs have significantly reduced stability or enhanced ISVP-to-ISVP* conversion *in vitro* (Fig 2B).

Conversion to ISVP* results in loss of outer capsid proteins that are essential for entry (27, 28). As a consequence, ISVPs that are heated to temperatures that result in ISVP* conversion have significantly reduced titers. Measuring thermal stability of ISVP infectivity, therefore, is an alternate method to evaluate the efficiency of ISVP* formation. T3D/T1L L3S2 and T3D ISVPs were heated to 40°C and loss of infectivity was measured by plaque assay. Consistent with previous work (20), at 40°C, most of the T3D ISVPs did not convert to ISVP* and the change in titer was minimal (Fig 2C). However, heating T3D/T1L L3S2 ISVPs to 40°C resulted in ISVP* conversion and a significant loss in infectivity (Fig 2C). These data indicate that the reovirus core proteins play a role in stability of the ISVP, a function previously not attributed to the major core proteins λ1 and σ2.

Enhanced ISVP-to-ISVP* conversion is not due to interactions with RNA. In addition to its structural functions, λ1 plays a variety of other roles during infection. One of those functions involves interaction with RNA (29, 30). If λ1-RNA interactions affect stability of the particles, it may explain why viruses with different core proteins and, consequently, the potential for different RNA interaction properties, may have altered stability. To rule out this possibility, we tested the ISVP-to-ISVP* conversion efficiency of genome-containing particles in comparison to genome-deficient particles of T3D. This comparison would allow us to uncover the contribution of viral genomic RNA to ISVP stability. ISVP-to-ISVP* conversion was again determined as a measure of trypsin sensitivity of μ1 δ. Stability of ISVPs of genome-containing particles and genome-deficient particles was not significantly different which suggests that λ1-RNA interactions do not affect ISVP-to-ISVP* conversion. Thus, the ISVP-to-ISVP* phenotype of T3D/T1L L3S2 is likely not related to differences in RNA interactions (Fig 3).

Isolation of heat resistant mutants in T3D/T1L L3S2. Because ISVP particles that have converted to ISVP* are less infectious, it is possible to select for and isolate variants with mutations that render ISVPs more stable and thus still retain infectivity after exposure to heat (28, 31, 32). Mapping such mutations could reveal key interactions between viral structural proteins that contribute to maintaining ISVP stability. In order to better understand the basis for the lower stability of this reassortant, we sought to identify such mutations in T3D/T1L L3S2 (Fig 4A). ISVPs of T3D/T1L L3S2 were heated to 40°C (a temperature at which they display significantly lower infectivity than that of similarly treated wild-type ISVPs derived from T3D) and subjected

to plaque assay. Resulting plaques were isolated as potential heat resistant mutants. To confirm the heat resistance of these isolates, ISVPs of each isolate were again incubated at 40°C and loss of infectivity in comparison to ISVPs incubated at 4°C was determined by plaque assay. Of the 20 isolates tested, 7 were determined to have little to no loss in infectivity. These isolates were considered to be heat resistant (HR) (Fig 4B). For each of these 7 isolates, genome segments encoding λ1, σ2, and μ1 (L3, S2 and M2 respectively) were sequenced. We reasoned that these genome segments will bear mutations because T3D/T1L L3S2 differs from T3D in the properties of λ1 and σ2, and because μ1 has been previously implicated in controlling stability of ISVPs (28, 33–35). None of the isolates contained mutations in L3 or S2. Four isolates were identified with mutations in μ1. HR16 had a mutation at amino acid 459 (lysine to glutamic acid) which is located in the δ fragment of μ1. HR2, HR15 and HR17 had mutations in the ϕ fragment of μ1. The mutation in HR 15 was at amino acid 607 (proline to glutamine) and HR2 and HR17 had the same mutation at amino acid 615 (alanine to threonine) (Fig 4 C, D, E). Notably, the K459E mutation has been previously identified as a stabilizing mutation (31). However, mutations in μ1 ϕ that contribute to ISVP stability or ISVP-to-ISVP* conversion efficiency have not been previously identified.

Mutations in μ1 stabilize T3D/T1L L3S2 ISVPs. Because we did not sequence the entire genome of HR viruses, it remains possible that mutations in genome segments other than L3, S2 and M2 influence the thermal stability of ISVPs generated from the second-site revertants. To evaluate the stabilizing effect of the identified mutations on T3D/T1L L3S2 ISVPs, each mutation was introduced individually into a T3D/T1L L3S2 background. Each new mutant virus was tested for ISVP-to-ISVP* conversion efficiency.

ISVPs of each virus were generated and incubated over a gradient of temperatures. ISVP* conversion was determined as a measure of trypsin sensitivity of the μ1 δ fragment (21). In comparison to T3D/T1L L3S2, each of the ISVPs with μ1 mutations had increased stability, suggesting that these amino acid residues in μ1 play important roles in ISVP-to-ISVP* conversion (Fig 5A). To verify these results, the infectivity of ISVPs of T3D/T1L L3S2 and each of the μ1 mutants at 4°C and 40°C was compared by plaque assay. Consistent with the results seen in Fig 2C, T3D/T1L L3S2 ISVPs experience a loss of infectivity at this temperature. In contrast, introduction of μ1 changes identified in heat resistant mutants into T3D/T1L L3S2 result in ISVP particles that display greater stability (Fig 5B). These data indicate that mutations in μ1 are sufficient to restore wild-type like ISVP-to-ISVP* conversion efficiency and thermal stability to T3D/T1L L3S2.

Mutations in μ1 also affect ISVP-to-ISVP* conversion in wild-type T3D. The μ1 mutations that restored thermal stability of ISVPs and normal ISVP-to-ISVP* conversion efficiency of T3D/T1L L3S2 are not in a position to contact proteins that make up the core (25, 36). Thus, it seems unlikely that these mutations stabilize the capsid by directly altering core-outer capsid interactions. One possibility is that the changes in μ1 simply stabilize the capsid by strengthening interactions between μ1 monomers or between μ1 trimers. If so, the μ1 mutations would be expected to further stabilize ISVPs of T3D, which contains different L3 and S2 alleles. To test this idea, we also generated viruses containing one of each of the three μ1 changes found in the HR viruses in a wild-type T3D background. As before, ISVPs of each virus were generated and incubated over a gradient of temperatures. ISVP* conversion was again determined as

a measure of trypsin sensitivity of the μ1 δ fragment. In comparison to wild-type T3D, each mutant underwent ISVP-to-ISVP* conversion much less efficiently (Fig 6A). To verify these results, each virus was tested for loss of infectivity. ISVPs of T3D along with each mutant were heated to 49°C and loss in infectivity was measured by plaque assay. The 49°C temperature was determined empirically as the lowest temperature at which T3D ISVPs exhibit a loss in infectivity (data not shown). Consistent with the data in Fig 6A, at this temperature each of the μ1 mutants displayed no loss of infectivity when compared to wild-type T3D. These data suggest that the mutations identified in μ1 are generally stabilizing mutations and not directly related to the effects of the mismatched core proteins.

Mismatches between the core and outer capsid proteins affect viral replication and transcription. To determine if the differences in the ISVP-to-ISVP* conversion efficiency of T3D and T3D/T1L L3S2 are relevant during a viral infection, we next examined viral growth via following infection of cells at an MOI of 0.1 PFU/cell. Virus titer at 24 h following infection was determined by plaque assay and viral yield was calculated as an increase in titer from 0 h post infection (which measured virus adsorbed to cells at the start of infection). We observed that infection with T3D/T1L L3S2 resulted in an increased yield in comparison to T3D (Fig 7A). To determine if this growth phenotype correlates with increased ISVP-to-ISVP* conversion efficiency, we tested the impact of introducing a representative μ1 mutation, A615T in these viruses. While growth of T3D was significantly higher than growth of T3D M2 A615T, growth of T3D/T1L L3S2 was not significantly different from T3D/T1L L3S2 M2A615T (Fig 7A). As the M2 A615T mutation in T3D/T1L L3S2 restores the stability of its ISVPs, these data

238 indicate that differences in replication efficiency of T3D and T3D/T1L L3S2 is not a
239 consequence of the capacity of the reassortant virus to more easily convert to ISVP*.
240 These data also suggest that T1L derived L3 and S2 genome segments can influence
241 the properties of T3D in multiple independent ways.

242 The higher replication potential of T3D/T1L L3S2 could be related to the capacity
243 of this virus to produce more viral gene products with faster kinetics or to a greater
244 extent. To test this idea, we next examined viral gene expression early during infection
245 using immunoblots. Cells were infected with ISVPs at an equal MOI and harvested at 0
246 or 10h post infection. Expression of the µ1 protein was assessed as a representative.
247 While expression of µ1 was visible at 10 h post infection in all samples, T3D/T1L L3S2
248 displayed significantly higher protein expression than WT T3D (Fig 7B). To test the
249 impact of ISVP-to-ISVP* conversion phenotypes on protein expression, we also
250 examined T3D M2 A615T and T3D/T1L L3S2 M2 A615T. While both viruses displayed
251 lower protein levels than T3D/T1L L3S2, the mutant in the T3D background had
252 significantly lower µ1 expression than the mutant in the T3D/T1L L3S2 suggesting that
253 the ISVP-to-ISVP* conversion phenotype alone is not responsible for the increase in
254 protein expression. To determine whether the greater level of viral protein expression is
255 a consequence of a higher level of viral mRNA, we measured transcription of viral S1
256 mRNA early during infection using RT-qPCR. Cells were infected with ISVPs at an
257 equal MOI and harvested at 6 hours post infection. At this timepoint, T3D/T1L L3S2
258 showed significantly greater reovirus S1 transcripts compared to T3D, indicating that the
259 increase in protein production is likely due to enhanced transcription by the reassortant

virus (Fig 7C). These data indicate that swapping core proteins between T1L and T3D in a reassortant virus also influence post-entry viral replication events.

DISCUSSION

To test the role of the inner core proteins on disassembly and early entry events we generated a reassortant virus with major core proteins from T1L and all other proteins (including the outer capsid) from T3D (T3D/T1L L3S2). T3D/T1L L3S2 undergoes ISVP-to-ISVP* conversion much more efficiently. We identified mutations in μ1 that stabilize ISVPs. T3D/T1L L3S2 also demonstrated increased growth kinetics compared to the parental T3D strain. Surprisingly, the more efficient growth of T3D/T1L L3S2 was not related to its capacity to undergo more efficient ISVP-to-ISVP* transition. Instead, increased growth of T3D/T1L L3S2 relates to more rapid protein and mRNA production early in infection. These data suggest that alteration in properties of core proteins can impact the function of the outer capsid proteins in cell entry. Additionally, properties of core proteins can also influence the enzymatic functions of the capsid that are required to establish efficient infection of host cells.

The reovirus core is a T=1 icosahedron and it is surrounded by the outer capsid (T=13). The outer capsid is made up of 200 heterohexamers of μ1 and σ3 proteins that cover the core (25, 36). It is penetrated by λ2 pentameric turrets at each five-fold axis of symmetry. Trimers of the σ1 attachment protein are situated inside these λ2 turrets (8, 25). The core is made up of 120 copies of λ1 arranged in asymmetric pairs of pentamers to form decamers. Twelve such decamers make up the core. The σ2 protein

clamps onto λ1 at 3 different sites within an asymmetric unit resulting in 150 copies of σ2 stabilizing the core shell (8). At each five-fold axis of symmetry, channels penetrate the shell via the λ2 pentameric turrets. It is at each of these channels that the λ3 polymerase interacts with λ1 and is thought to interact with the polymerase co-factor μ2 (5, 37, 38). There are no known contacts between λ1 and the outer capsid. A majority of contacts between the core and the outer capsid occur between μ1 and σ2. These interactions involve the bottom surface of μ1 and the top surface of σ2 (25). The “hub and spoke” structure formed by the C-terminal 33 residue s of μ1 which is thought to be important for stabilizing the μ1 lattice also makes contact with λ2 and/or σ2 (25). This interaction is thought to be stabilized in part by the μ1 residues 51-62 which form flexible loops (25). It is possible that the polymorphic differences between σ2 proteins of T1L and T3D influence interaction with μ1 sufficiently enough such that disassembly is altered. λ1 can also impact interaction of the core with μ1, thereby changing disassembly. However, because μ1 does not contact λ1, this effect would occur indirectly if the structure or conformation of λ2 or σ2, two proteins that do interact with μ1, is altered due to differences in λ1 residues. The relative contribution of differences in properties of σ2 and λ1and the potential subtle differences in structure remain the focus of our ongoing work.

Differences in entry efficiency between different serotypes and laboratory strains of reovirus along with genetic approaches have been used to study how conformational changes and cleavage events required for entry are regulated. Panels of reassortant viruses link differences in ISVP-to-ISVP* conversion to μ1 (28). The autocatalytic cleavage of μ1 and efficiency of ISVP* formation have both been linked to distinct

305 portions of the δ fragment of μ1 (33). Multiple other studies have linked efficiency of
306 entry related disassembly events to the δ fragment of μ1 (31, 33, 35, 36, 39). The μ1N
307 fragment is released from the particle during ISVP* conversion and the released
308 fragment is thought to function in a positive feedback loop to further drive ISVP*
309 conversion (40). The ISVP* promoting activity of μ1N is most efficient in presence of
310 membranes, likely because membrane associated μ1N recruits ISVP-like particles (41,
311 42). Cleavage of ϕ, which is required for its release from particles during ISVP*
312 conversion is also required for efficient interaction of ISVPs with membranes (42).
313 However, precisely how ϕ functions in this step is not known. Here, we have identified
314 two mutations in the ϕ fragment of μ1 that influence ISVP-to-ISVP* conversion. These
315 mutations are the first indication that the ϕ fragment may also be involved in ISVP-to-
316 ISVP* conversion efficiency. Because our ISVP-to-ISVP* reactions were performed in
317 absence of membranes, the mutations are unlikely to influence ISVP-to-ISVP*
318 conversion by affecting particle-membrane interaction. Thus, the precise mechanism by
319 which the identified ϕ residues influence ISVP* remains unclear. While the majority of
320 μ1-σ3 interactions occur in the jelly-roll domains (residues 306-514) of μ1, both of the
321 mutations identified are in a region proposed to form the cradle for the base of σ3 (36)
322 This region has not been shown to interact with any core proteins or with neighboring μ1
323 monomers (36). Therefore, it is unlikely that these mutations stabilize ISVPs by
324 strengthening inter- or intra- μ1 trimer interactions or by interacting with core proteins.
325 The identified mutations are in a region of μ1 that may unfold in order to accommodate
326 μ1N release which is a necessary step of ISVP-to-ISVP* conversion (25, 36). Thus, one
327 likely explanation is that ϕ properties affect the release of μ1N.

The L3 gene segment encoded λ1 protein is thought of first as a structural protein that makes up the inner core of reovirus. However, as is the case with most viruses, proteins are capable of playing multiple roles during infection. In addition to its structural roles λ1 has RNA helicase activity, phosphohydrolase activity and is known to interact with RNA (30). The role of each of these functions during infection is currently unknown. The polymerase λ3 interacts with λ1 on the inside of the shell at each five-fold axis (8, 43). While the position of the transcription cofactor protein μ2 within the capsid is not known, it is possible that it also interacts with λ1. Thus, the interaction of λ1 with these encapsidated enzymes could alter viral transcription efficiency. Reovirus serotypes T1L and T3D replicate with different efficiency in some cell lines, with T1L replicating to a higher extent and with faster kinetics (44). Reassortant analyses have partially linked this phenotype to the T1L derived λ1-encoding L3 gene segment (44). Our studies indicate that the enhanced infection efficiency of T3D/T1L L3S2 is not related to its greater propensity for ISVP-to-ISVP* transition. Instead, we propose that enhanced efficiency of infection is a result of differences in the activity of λ1 itself or its impact on the activity of the transcriptional machinery comprised of λ3 and μ2. While the role of σ2 as a structural protein is well established, additional roles in replication have not been confidently identified. It has weak interactions with dsRNA and reassortant studies have linked σ2 with increased induction and sensitivity to interferon in some cell types (45, 46). Additional studies are needed with monoreassortants bearing only S2 and L3 gene segments in the T3D background to precisely ascertain the basis for the enhanced replicative efficiency of T3D/T1L L3S2.

Recent studies from our laboratory have revealed that reassortant viruses display phenotypes that are unexpected and extend beyond the known function of the protein. First, we found that, even though the primary function of the M2 encoded protein μ1 is in membrane penetration, an M2 reassortant virus displays greater attachment to host cells (47). Second, we found that though the S1 encoded σ1 protein is the attachment factor, an S1 reassortant impacts the stability of the μ1 layer with which it makes no interactions (20). Our current study presented here reveals that core proteins, previously only thought to have a structural role in packaging the genomic material, influence cell entry events regulated by the outer capsid. Until the advent of reverse genetics, reassortant analyses have been used as the main strategy to assign function to proteins of segmented viruses. This approach has also been useful to determine the genetic basis of viral disease. While this approach has been invaluable, we think our work suggests that the structure-function explanation of some phenotypes reported for reovirus and possibly other members of the *Reoviridae* family may be more complicated than previously appreciated.

MATERIALS AND METHODS

Cells and viruses. Spinner adapted murine L929 (L) cells were grown at 37°C in Joklik's minimal essential medium (Lonza) supplemented with 5% fetal bovine serum (FBS) (Life Technologies), 2 mM L-glutamine (Invitrogen), 100 U/ml penicillin (Invitrogen), 100 μg/ml streptomycin (Invitrogen), and 25 ng/ml amphotericin B (Sigma-Aldrich). All virus strains used in this study were derived from reovirus type 3 Dearing (T3D) and reovirus type 1 Lang (T1L) and were generated by plasmid-based reverse

373 genetics (48). Mutations within the T3D M2 gene were generated by QuikChange site-
374 directed mutagenesis (Agilent Technologies). Primer sequences are available upon
375 request.

376 **Virus propagation and purification**. All wild-type and mutant viruses used in this study
377 were propagated and purified as previously described (49, 50). Briefly, plaques isolated
378 from plasmid based reverse genetics were propagated successively in T-25, T75 and T-
379 175 flasks to generate P0, P1 and P2 virus stocks respectively. To generate purified
380 virus, L cells infected with P2 reovirus stocks were lysed by sonication. Virus particles
381 were extracted from the lysates using Vertrel-XF specialty fluid (Dupont) (51). The
382 extracted particles were layered onto 1.2- to 1.4-g/cm_3 CsCl step gradients. The
383 gradients were then centrifuged at 187,000 × *g* for 4 h at 4°C. Bands corresponding to
384 purified virus particles (~1.36 g/cm_3) (52) were isolated and dialyzed into virus storage
385 buffer (10 mM Tris, pH 7.4, 15 mM $MgCl_2$, and 150 mM NaCl). Following dialysis, the
386 particle concentration was determined by measuring the optical density of the purified
387 virus stocks at 260 nm (OD_{260}) (1 unit at OD_{260} is equal to 2.1 × 10_{12} particles/ml)

388 **Generation of ISVPs**. Purified virions of the indicated virus strains (2 × 10_{12} particles/ml
389 or 4 × 10_{12} particles/ml) were digested with 200 µg/ml TLCK (*N*α-*p*-tosyl-L-lysine
390 chloromethyl ketone)-treated chymotrypsin (Worthington Biochemical) in a total volume
391 of 100 µl for 1 hour at 32°C. After 1 h, the reaction mixtures were incubated for 20 min
392 on ice and quenched by the addition of 1 mM phenylmethylsulfonyl fluoride (Sigma-
393 Aldrich). The generation of ISVPs was confirmed by SDS-PAGE and Coomassie
394 brilliant blue staining.

Analysis of ISVP-ISVP* conversion. ISVPs ($2 \times 10_{12}$ particles/ml) of the indicated viral strains were divided into aliquots of equivalent volumes and heated at the indicated temperatures for 20 min. The reaction mixtures were cooled on ice and then digested with 0.10 mg/ml trypsin (Sigma-Aldrich) for 30 min on ice. Following addition of the SDS-PAGE loading dye, the samples subjected to SDS-PAGE analysis. For analysis by quantitative infectivity assay, P2 stocks or purified virus stocks of the indicated viruses were diluted 1:10 in virion storage buffer (10 mM Tris, pH 7.4, 15 mM $MgCl_2$, and 150 mM NaCl). 200µg/mL TLCK (*N*α-*p*-tosyl-L-lysine chloromethyl ketone)-treated chymotrypsin (Worthington Biochemical) was added to each sample. Samples were heated to 37°C for 30 min. The reaction was quenched by the addition of 1 mM phenylmethylsulfonyl fluoride (Sigma-Aldrich) and cooled on ice for 10 min. The reactions were divided in equivalent volumes and incubated at 4°C or 40°C for 20 min. Reactions were used to initiate infection of L929 cells and infectivity was determined by plaque assay. The change in infectivity at a given temperature (*T*) was calculated using the following formula: $\log_{10}(\text{PFU/ml})_T - \log_{10}(\text{PFU/ml})_{4°C}$.

Analysis of virion stability. Virions ($2x10_{12}$ particles/ml) of the indicated viral strains were divided into aliquots of equivalent volumes and heated at the indicated temperatures for 20 min. The reaction mixtures were cooled on ice and then digested with 0.10 mg/ml trypsin (Sigma-Aldrich) for 30 min on ice. Following addition of SDS loading dye, the samples were subjected to analysis by SDS-PAGE.

Isolation and verification of heat resistant (HR) mutants. ISVPs of purified T3D/T1L L3S2 were generated and subsequently heated to 40°C for 20 min. Resulting reactions were diluted in phosphate-buffered saline (PBS) supplemented with 2 mM $MgCl_2$ and

subjected to plaque assay. Heat resistant mutants were selected by plaque purification and propagated in L cells to obtain P0 viral stocks. P0 stocks were diluted 1:10 in virion storage buffer (10 mM Tris, pH 7.4, 15 mM $MgCl_2$, and 150 mM NaCl). 200µg/mL TLCK (*N*α-*p*-tosyl-L-lysine chloromethyl ketone)-treated chymotrypsin (Worthington Biochemical, Lakewood, NJ) was added to each sample. Samples were heated to 37°C for 30 min. The reaction was quenched by the addition of 1 mM phenylmethylsulfonyl fluoride (Sigma-Aldrich) and cooled on ice for 10 min. The reactions were divided in equivalent volumes and incubated at 4°C or 40°C for 20 min. Reactions were used to initiate infection of L929 cells and infectivity was determined by plaque assay. The change in infectivity at a given temperature (*T*) was calculated using the following formula: $\log_{10}(\text{PFU/ml})_T - \log_{10}(\text{PFU/ml})_{4°C}$.

Plaque titration. Plaque assays were conducted in spinner-adapted L929 cells plated in 6-well plates (Greiner Bio-One). Cells were adsorbed with dilutions of virus in phosphate-buffered saline (PBS). Cells were overlaid with a molten mixture comprised of 1× medium 199 and 1% Bacto agar supplemented with 10 µg/ml chymotrypsin. Five days following infection, the monolayers were fixed by addition of 4% formaldehyde solution in PBS and incubated overnight. The agar overlay was peeled off, and the monolayers were stained with 1% crystal violet stain in 5% ethanol for 5 h at room temperature. The monolayers were washed with water. Virus titer was quantified by manual counting of plaques.

Analysis of protein levels by immunoblotting. The samples were whole-cell lysates of infected cells prepared using radioimmunoprecipitation assay (RIPA) lysis buffer (50 mM NaCl, 1 mM EDTA at pH 8, 50 mM Tris at pH 7.5, 1% Triton X-100, 1% sodium

441 deoxycholate, 0.1% SDS) supplemented with protease inhibitor cocktail (Roche) and
442 500 μM PMSF, and they were resolved on 10% SDS-PAGE gels and transferred to
443 nitrocellulose membranes. For immunoblotting using polyclonal rabbit antireovirus
444 serum, the membranes were blocked with 5% milk in Tris-buffered saline (TBS) at room
445 temperature for 1 h. Following blocking, rabbit anti-reovirus serum (1:1,000) or anti-
446 PSTAIR was incubated with the membrane in appropriate blocking buffer at room
447 temperature for 1 h. The membranes were washed with TBS supplemented with 0.1%
448 Tween 20 (TBS-T) twice for 15 min and then incubated with Alexa Fluor-conjugated
449 anti-rabbit IgG or anti-mouse IgG in blocking buffer. Following three washes,
450 membranes were scanned using an Odyssey infrared imager (LI-COR), and intensities
451 of bands were quantified using Image Studio Lite software (LI-COR).

452 **Analysis of mRNA levels by RT-qPCR**. RNA was extracted from infected cells, at
453 various times after infection, using a total RNA minikit (Bio-Rad). For RT-qPCR, 0.5 to 2 μg
454 of RNA was reverse transcribed with the high-capacity cDNA RT kit (Applied Biosystems),
455 using random hexamers for amplification of cellular and viral genes. Undiluted cDNA was
456 subjected to PCR using SYBR Select Master Mix (Applied Biosystems) and primers specific
457 for T3D S1 and GAPDH. Fold increases in gene expression with respect to control samples
458 (indicated in figure legend) were measured using the $\Delta\Delta C_T$ method (53). Calculations for
459 determining $\Delta\Delta C_T$ values and relative levels of gene expression were performed as follows:
460 fold increase in viral gene expression = $2_{[-(\Delta\Delta CT)]}$

461 **Statistical analyses.** The reported values represent the means of three independent
462 biological replicates. The error bars indicate standard deviations (SD). *P* values were
463 calculated using Student's *t* test (two-tailed; unequal variance assumed).

Modeling. Molecular graphics were created and analysis were performed with the UCSF Chimera package (54).

FIGURE LEGENDS

Figure 1. Schematic representation of reovirus capsid proteins.

Figure 2. T3D/T1L L3S2 exhibits increased efficiency of ISVP to ISVP* conversion *in vitro*. (A) T3D and T3D/T1L L3S2 virions ($2x10_{12}$ particles/ml) were divided into aliquots of equal volume and incubated at either 4°C or over a range of temperatures (65-85°C) for 5 min. The reactions were chilled on ice and digested with 0.10mg/ml trypsin for 30 min. Following addition of loading dye, the samples were subjected to SDS-PAGE analysis. The positions of major capsid proteins are shown. µ1 runs as µ1C (15). (B) ISVPs ($2x10_{11}$ particles/ml) of T3D or T3D/T1L L3S2 were divided into aliquots of equivalent volume and incubated either at 4°C or over a range of temperatures (22-42°C) for 20 min. The reactions were chilled on ice and digested with 0.10 mg/ml trypsin for 30 min. Following addition of loading dye the samples were subjected to SDS-PAGE analysis. The gels shown are representative of at least 3 independent experiments. The position of major capsid proteins is shown. µ1 runs as µ1C. (C) ISVPs generated from P2 stocks of the indicated virus strain were divided into aliquots of equivalent volume and incubated at either 4°C or 40°C for 20 min. Reactions were then diluted in PBS and subjected to plaque assay. The data are plotted as mean loss of infectivity for three

485 independent samples in comparison to samples incubated at 4°C. Error bars indicate
486 SD. *, P<0.05 as determined by student's t-test in comparison to T3D.

487 **Figure 3.** Increased ISVP to ISVP* efficiency in T3D/T1L L3S2 is not due to altered
488 interactions with viral RNA. ISVPs ($2x10_{11}$ particles/ml) derived from genome-containing
489 or genome-deficient particles of strain T3D were divided into aliquots of equivalent
490 volume and incubated at either 4°C or over a range of temperatures (22-40°C) for 20
491 min. The reactions were chilled on ice and digested with 0.10 mg/ml trypsin for 30 min.
492 Following addition of loading dye the samples were subjected to SDS-PAGE analysis.
493 The position of major capsid proteins is shown. µ1 runs as µ1C.

494 **Figure 4.** Selection of viruses with mutations that confer stability to T3D/T1L L3S2
495 ISVPs. (A) Diagram depicting the process for selecting for mutants with reduced ISVP-
496 ISVP* conversion efficiency of T3D/T1L L3S2. ISVPs of T3D/T1L L3S2 were incubated
497 at 40°C for 20 min. Reactions were then diluted in PBS and subjected to plaque assay.
498 Viruses from resulting plaques were isolated and propagated to generate P0 stocks.
499 Heat resistance of these putative heat resistant (HR) plaque isolates was confirmed by
500 measuring the thermal stability of ISVPs incubated at 4°C or 40°C using a plaque
501 assay. Mutants that were confirmed as heat resistant were sequenced. (B) ISVPs
502 generated from P0 stocks were incubated at either 4°C or 40°C for 20 min. Reactions
503 were then diluted in PBS and subjected to plaque assay. ND, Not detectable. (C, D) Top
504 (left) and side (right) views of µ1 trimer (C) and monomer (D) are shown. Position of
505 mutations identified in HR viruses are shown in green. µ1 cleavage fragments are
506 colored as indicated (E) with one µ1 monomer shown with darker colors.

Figure 5. Mutations in µ1 restore stability. (A) ISVPs ($2x10_{11}$ particles/ml) of T3D/T1L L3S2 with the indicated M2 mutations were divided into aliquots of equivalent volume and incubated at either 4°C or over a range of temperatures (22-42°C) for 20 min. The reactions were chilled on ice and digested with 0.10 mg/ml trypsin for 30 min. Following addition of loading dye the samples were subjected to SDS-PAGE analysis. The gels shown are representative of at least 3 independent experiments. The position of major capsid proteins is shown. µ1 runs as µ1C. (B) ISVPs generated from P2 stocks of the indicated virus strain were divided into aliquots of equivalent volume and incubated at either 4°C or 40°C for 20 min. Reactions were then diluted in PBS and subjected to plaque assay. The data are plotted as mean loss of infectivity for three independent samples in comparison to samples incubated at 4°C. Error bars indicate SD. **, $P<0.01$, ***, $P<0.001$ as determined by student's t-test in comparison to T3D/T1L L3S2.

Figure 6. Mutations in µ1 hyperstabilize T3D. (A) ISVPs ($2x10_{11}$ particles/ml) of T3D and T3D with the indicated M2 mutations were divided into aliquots of equivalent volume and incubated at either 4°C or over a range of temperatures (32-46°C) for 20 min. The reactions were chilled on ice and digested with 0.10 mg/ml trypsin for 30 min. Following addition of loading dye the samples were subjected to SDS-PAGE analysis. The gels shown are representative of at least 3 independent experiments. The position of major capsid proteins is shown. µ1 runs as µ1C. (B) ISVPs generated from purified virions were divided into aliquots of equivalent volume and incubated at either 4°C or 42°C for 20 min. Reactions were then diluted in PBS and subjected to plaque assay. The data are plotted as mean loss of infectivity for three independent samples in

529 comparison to samples incubated at 4°C. Error bars indicate SD. ***, P<0.001, **,
530 P<0.01 as determined by student's T-test in comparison to T3D.

531

532 **Figure 7**. T3D/T1L L3S2 affects viral replication. (A) L cell monolayers were infected
533 with T3D or T3D/T1L L3S2 or with the indicated mutant viruses at an MOI of 0.1
534 PFU/cell. At 0h and 24h post infection, the infected cells were lysed and the viral yield
535 was quantified by plaque assay. Error bars indicate SD. *, P<0.05, ***, P<0.001 as
536 determined by student's t-test in comparison to T3D. (B) L cell monolayers were
537 infected with the indicated viruses at an MOI of 10 PFU/cell. At 10h post infection, the
538 cells were lysed and protein production was determined by immunoblotting. Protein
539 quantification of 3 replicates normalized to PSTAIR is shown. Error bars indicate SD. **,
540 P<0.01, ***, P<0.001 as determined by student's t-test in comparison to T3D. (C) L cell
541 monolayers were infected with the indicated viruses at an MOI of 10 PFU/cell. At the
542 indicated times post infection, the cells were lysed and total RNA was isolated. cDNA
543 was generated using primers for T3D S1 and GAPDH. mRNA production was measured
544 by qPCR. Data shown are represented as fold change compared to mock infected
545 samples and normalized to GAPDH. Error bars indicate SD. ***, P<0.001 as
546 determined by student's t-test in comparison to T3D

547

548

549

REFERENCES

1. SABIN AB. 1959. Reoviruses. A new group of respiratory and enteric viruses formerly classified as ECHO type 10 is described. Science 130:1387–1389.

2. Gomatos PJ, Tamm I. 1963. THE SECONDARY STRUCTURE OF REOVIRUS RNA. Proc Natl Acad Sci U S A 49:707–714.

3. Bellamy AR, Shapiro L, August JT, Joklik WK. 1967. Studies on reovirus RNA. I. Characterization of reovirus genome RNA. J Mol Biol 29:1–17.

4. Dermody TS, Parker JSL, Sherry B. 2013. Orthoreoviruses, p 1304–1346. Fields virology. Lippincott Williams & Wilkins, Philadelphia, PA.

5. Gillies S, Bullivant S, Bellamy AR. 1971. Viral RNA Polymerases: Electron Microscopy of Reovirus Reaction Cores. Science (80-) 174:694 LP – 696.

6. Skehel JJ, Joklik WK. 1969. Studies on the in vitro transcription of reovirus RNA catalyzed by reovirus cores. Virology 39:822–31.

7. Liemann S, Chandran K, Baker TS, Nibert ML, Harrison SC. 2002. Structure of the reovirus membrane-penetration protein, μ1, in a complex with its protector protein, σ3. Cell 108:283–295.

8. Reinisch KM, Nibert ML, Harrison SC. 2000. Structure of the reovirus core at 3.6 Å resolution. Nature 404:960–967.

9. Mao ZX, Joklik WK. 1991. Isolation and enzymatic characterization of protein lambda 2, the reovirus guanylyltransferase. Virology 185:377–386.

10. Baer GS, Dermody TS. 1997. Mutations in reovirus outer-capsid protein sigma3

selected during persistent infections of L cells confer resistance to protease inhibitor E64. J Virol 71:4921–4928.

11. Silverstein SC, Astell C, Levin DH, Schonberg M, Acs G. 1972. The mechanisms of reovirus uncoating and gene activation in vivo. Virology 47:797–806.

12. Dryden KA, Wang G, Yeager M, Nibert ML, Coombs KM, Furlong DB, Fields BN, Baker TS. 1993. Early steps in reovirus infection are associated with dramatic changes in supramolecular structure and protein conformation: analysis of virions and subviral particles by cryoelectron microscopy and image reconstruction. J Cell Biol 122:1023–1041.

13. Nibert ML, Fields BN. 1992. A carboxy-terminal fragment of protein mu 1/mu 1C is present in infectious subvirion particles of mammalian reoviruses and is proposed to have a role in penetration. J Virol 66:6408–6418.

14. Borsa J, Sargent MD, Lievaart PA, Copps TP. 1981. Reovirus: evidence for a second step in the intracellular uncoating and transcriptase activation process. Virology 111:191–200.

15. Nibert ML, Odegard AL, Agosto MA, Chandran K, Schiff LA. 2005. Putative autocleavage of reovirus mu1 protein in concert with outer-capsid disassembly and activation for membrane permeabilization. J Mol Biol 345:461–474.

16. Odegard AL, Chandran K, Zhang X, Parker JSL, Baker TS, Nibert ML. 2004. Putative autocleavage of outer capsid protein micro1, allowing release of myristoylated peptide micro1N during particle uncoating, is critical for cell entry by reovirus. J Virol 78:8732–8745.

593 17. Zhang L, Chandran K, Nibert ML, Harrison SC. 2006. Reovirus mu1 structural
594 rearrangements that mediate membrane penetration. J Virol2006/09/27.
595 80:12367–12376.

596 18. Chandran K, Farsetta DL, Nibert ML. 2002. Strategy for nonenveloped virus entry:
597 a hydrophobic conformer of the reovirus membrane penetration protein micro 1
598 mediates membrane disruption. J Virol 76:9920–33.

599 19. Snyder AJ, Wang JC-Y, Danthi P. 2019. Components of the Reovirus Capsid
600 Differentially Contribute to Stability. J Virol 93:e01894-18.

601 20. Thete D, Danthi P. 2018. Protein mismatches caused by reassortment influence
602 functions of the reovirus capsid. bioRxiv.

603 21. Snyder AJ, Wang JC-Y, Danthi P. 2018. The reovirus μ1 protein contributes to the
604 environmental stability of virions. bioRxiv.

605 22. Harrison SJ, Farsetta DL, Kim J, Noble S, Broering TJ, Nibert ML. 1999.
606 Mammalian reovirus L3 gene sequences and evidence for a distinct amino-
607 terminal region of the lambda1 protein. Virology 258:54–64.

608 23. Xu W, Coombs KM. 2009. Conserved structure/function of the orthoreovirus major
609 core proteins. Virus Res 144:44–57.

610 24. Chapell JD, Goral MI, Rodgers SE, dePamphilis CW, Dermody TS. 1994.
611 Sequence diversity within the reovirus S2 gene: reovirus genes reassort in nature,
612 and their termini are predicted to form a panhandle motif. J Virol 68:750–756.

613 25. Zhang X, Ji Y, Zhang L, Harrison SC, Marinescu DC, Nibert ML, Baker TS. 2005.

614 Features of reovirus outer capsid protein mu1 revealed by electron
615 cryomicroscopy and image reconstruction of the virion at 7.0 Angstrom resolution.
616 Structure 13:1545–1557.

617 26. Snyder AJ, Danthi P. 2018. Infectious Subviral Particle to Membrane Penetration
618 Active Particle (ISVP-to-ISVP*) Conversion Assay for Mammalian Orthoreovirus.
619 Bio-protocol 8:e2700.

620 27. Snyder AJ, Danthi P. 2015. Lipid Membranes Facilitate Conformational Changes
621 Required for Reovirus Cell Entry. J Virol 90:2628–2638.

622 28. Middleton JK, Severson TF, Chandran K, Gillian AL, Yin J, Nibert ML. 2002.
623 Thermostability of reovirus disassembly intermediates (ISVPs) correlates with
624 genetic, biochemical, and thermodynamic properties of major surface protein
625 mu1. J Virol 76:1051–61.

626 29. Lemay G, Danis C. 1994. Reovirus λ1 protein: Affinity for double-stranded nucleic
627 acids by a small amino-terminal region of the protein independent from the zinc
628 finger motif. J Gen Virol 75:3261–3266.

629 30. Bisaillon M, Bergeron J, Lemay G. 1997. Characterization of the nucleoside
630 triphosphate phosphohydrolase and helicase activities of the reovirus λ1 protein. J
631 Biol Chem 272:18298–18303.

632 31. Middleton JK, Agosto MA, Severson TF, Yin J, Nibert ML. 2007.
633 Thermostabilizing mutations in reovirus outer-capsid protein mu1 selected by heat
634 inactivation of infectious subvirion particles. Virology2007/01/17. 361:412–425.

635 32. Agosto MA, Middleton JK, Freimont EC, Yin J, Nibert ML. 2007. Thermolabilizing
636 Pseudoreversions in Reovirus Outer-Capsid Protein μ1 Rescue the Entry Defect
637 Conferred by a Thermostabilizing Mutation. J Virol 81:7400 LP – 7409.

638 33. Sarkar P, Danthi P. 2010. Determinants of strain-specific differences in efficiency
639 of reovirus entry. J Virol 84:12723–12732.

640 34. Drayna D, Fields BN. 1982. Biochemical studies on the mechanism of chemical
641 and physical inactivation of reovirus. J Gen Virol 63 (Pt 1):161–170.

642 35. Wessner DR, Fields BN. 1993. Isolation and genetic characterization of ethanol-
643 resistant reovirus mutants. J Virol 67:2442–2447.

644 36. Liemann S, Chandran K, Baker TS, Nibert ML, Harrison SC. 2002. Structure of
645 the reovirus membrane-penetration protein, Mu1, in a complex with is protector
646 protein, Sigma3. Cell 108:283–295.

647 37. Farsetta DL, Chandran K, Nibert ML. 2000. Transcriptional activities of reovirus
648 RNA polymerase in recoated cores. Initiation and elongation are regulated by
649 separate mechanisms. J Biol Chem 275:39693–39701.

650 38. McDonald SM, Tao YJ, Patton JT. 2009. The ins and outs of four-tunneled
651 Reoviridae RNA-dependent RNA polymerases. Curr Opin Struct Biol2009/11/14.
652 19:775–782.

653 39. Hooper JW, Fields BN. 1996. Role of the mu 1 protein in reovirus stability and
654 capacity to cause chromium release from host cells. J Virol 70:459–467.

655 40. Agosto MA, Myers KS, Ivanovic T, Nibert ML. 2008. A positive-feedback

mechanism promotes reovirus particle conversion to the intermediate associated with membrane penetration. Proc Natl Acad Sci U S A 105:10571–6.

41. Snyder AJ, Danthi P. 2016. Lipids Cooperate with the Reovirus Membrane Penetration Peptide to Facilitate Particle Uncoating. J Biol Chem2016/11/15. 291:26773–26785.

42. Ivanovic T, Agosto MA, Zhang L, Chandran K, Harrison SC, Nibert ML. 2008. Peptides released from reovirus outer capsid form membrane pores that recruit virus particles. EMBO J 27:1289–98.

43. Zhang X, Walker SB, Chipman PR, Nibert ML, Baker TS. 2003. Reovirus polymerase λ3 localized by cryo-electron microscopy of virions at a resolution of 7.6 Å. Nat Struct Mol Biol 10:1011–1018.

44. Simon EJ, Howells MA, Stuart JD, Boehme KW. 2017. Serotype-specific killing of large cell carcinoma cells by reovirus. Viruses 9.

45. Dermody TS, Schiff LA, Nibert ML, Coombs KM, Fields BN. 1991. The S2 gene nucleotide sequences of prototype strains of the three reovirus serotypes: characterization of reovirus core protein sigma 2. J Virol 65:5721–5731.

46. Sherry B, Torres J, Blum MA. 1998. Reovirus induction of and sensitivity to beta interferon in cardiac myocyte cultures correlate with induction of myocarditis and are determined by viral core proteins. J Virol 72:1314–23.

47. Thete D, Danthi P. 2015. Conformational changes required for reovirus cell entry are sensitive to pH. Virology 483:291–301.

677 48. Boehme KW, Ikizler M, Kobayashi T, Dermody TS. 2011. Reverse genetics for
678 mammalian reovirus. Methods 55:109–113.

679 49. Sarkar P, Danthi P. 2010. Determinants of strain-specific differences in efficiency
680 of reovirus entry. J Virol2010/10/13. 84:12723–12732.

681 50. Furlong DB, Nibert ML, Fields BN. 1988. Sigma 1 protein of mammalian
682 reoviruses extends from the surfaces of viral particles. J Virol 62:246–256.

683 51. Mendez II, Hermann LL, Hazelton PR, Coombs KM. 2000. A comparative analysis
684 of freon substitutes in the purification of reovirus and calicivirus. J Virol Methods
685 90:59–67.

686 52. Smith RE, Zweerink HJ, Joklik WK. 1969. Polypeptide components of virions, top
687 component and cores of reovirus type 3. Virology 39:791–810.

688 53. Schmittgen TD, Livak KJ. 2008. Analyzing real-time PCR data by the comparative
689 C(T) method. Nat Protoc 3:1101–1108.

690 54. Pettersen EF, Goddard TD, Huang CC, Couch GS, Greenblatt DM, Meng EC,
691 Ferrin TE. 2004. UCSF Chimera--a visualization system for exploratory research
692 and analysis. J Comput Chem 25:1605–1612.

693

694

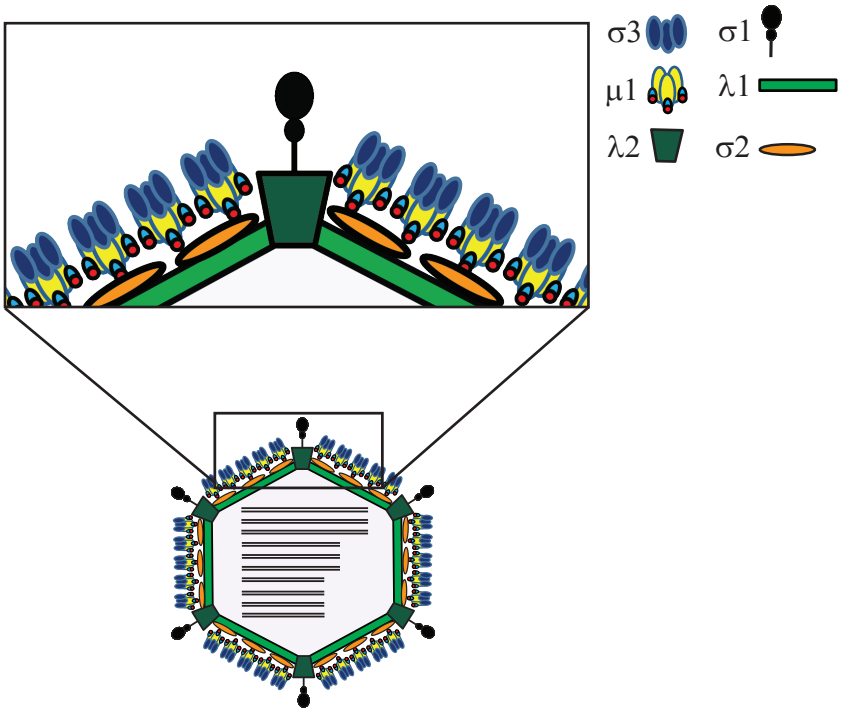

Figure 1. Schematic representation of reovirus capsid proteins.

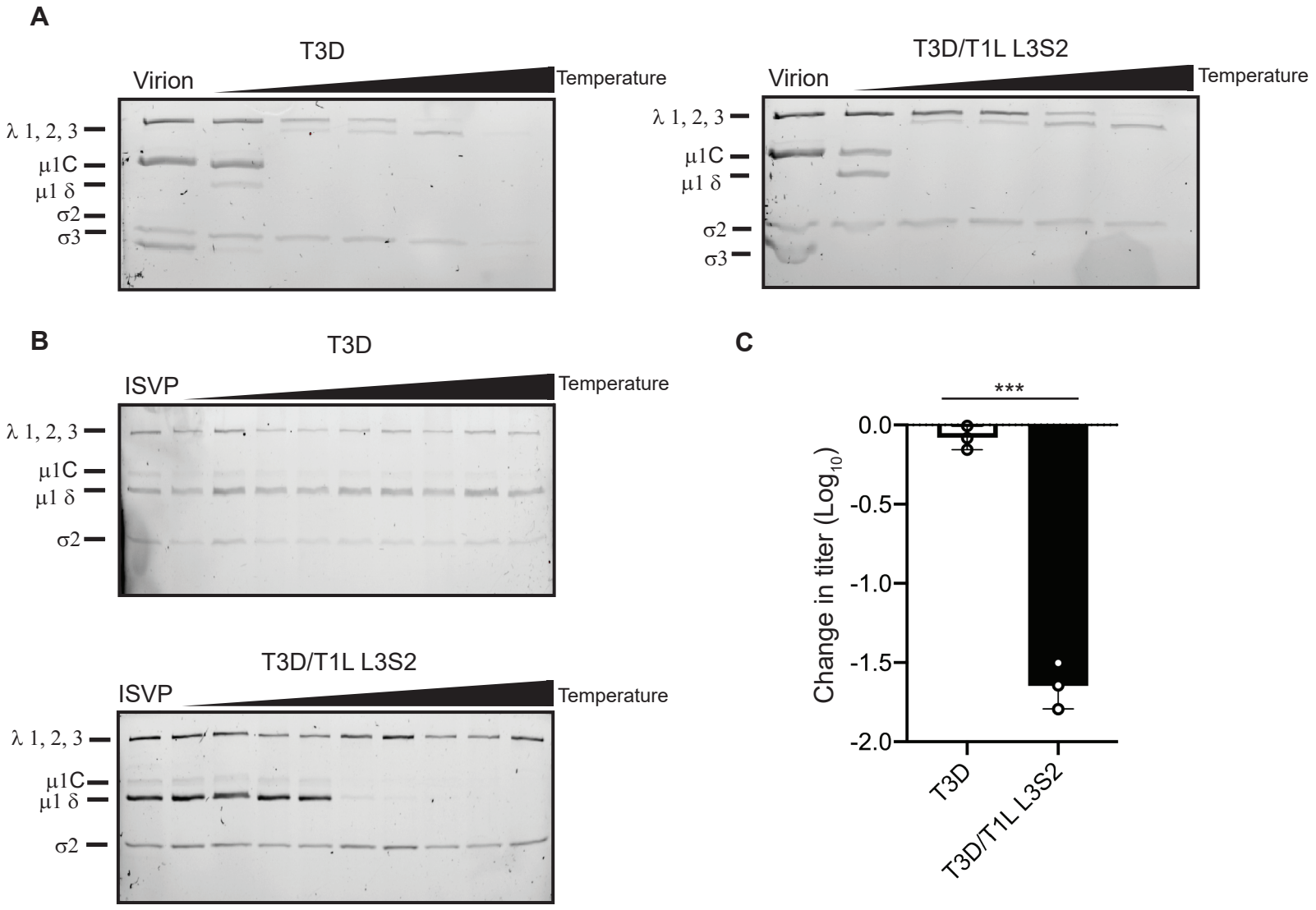

Figure 2. T3D/T1L L3S2 exhibits increased efficiency of ISVP to ISVP* conversion in vitro. (A) T3D and T3D/T1L L3S2 virions ($2x10^{12}$ particles/ml) were divided into aliquots of equal volume and incubated at either 4°C or over a range of temperatures (65-85°C) for 5 min. The reactions were chilled on ice and digested with 0.10mg/ml trypsin for 30 min. Following addition of loading dye, the samples were subjected to SDS-PAGE analysis. The positions of major capsid proteins are shown. μ1 runs as μ1C (15). (B) ISVPs ($2x10^{11}$ particles/ml) of T3D or T3D/T1L L3S2 were divided into aliquots of equivalent volume and incubated either at 4°C or over a range of temperatures (22-42°C) for 20 min. The reactions were chilled on ice and digested with 0.10 mg/ml trypsin for 30 min. Following addition of loading dye the samples were subjected to SDS-PAGE analysis. The gels shown are representative of at least 3 independent experiments. The position of major capsid proteins is shown. μ1 runs as μ1C. (C) ISVPs generated from P2 stocks of the indicated virus strain were divided into aliquots of equivalent volume and incubated at either 4°C or 40°C for 20 min. Reactions were then diluted in PBS and subjected to plaque assay. The data are plotted as mean loss of infectivity for three independent samples in comparison to samples incubated at 4°C. Error bars indicate SD. *, $P<0.05$ as determined by student's t-test in comparison to T3D.

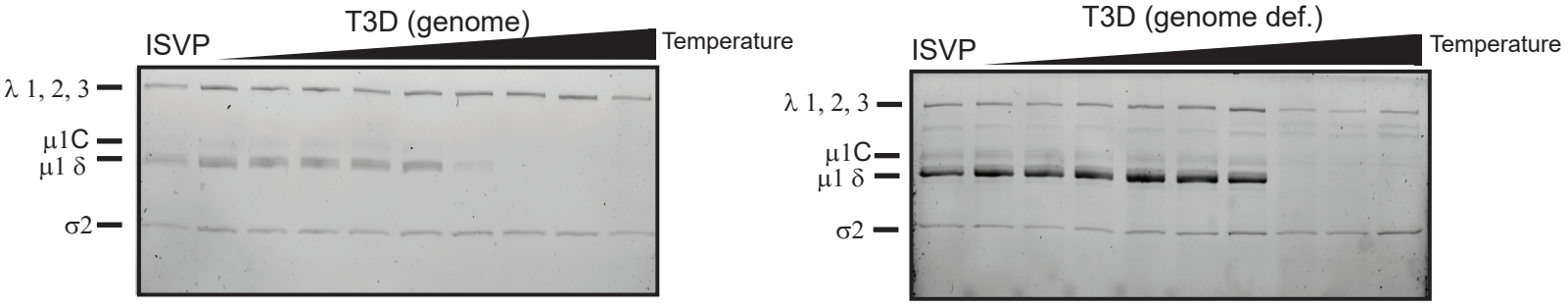

Figure 3. Increased ISVP to ISVP* efficiency in T3D/T1L L3S2 is not due to altered interactions with viral RNA. ISVPs ($2x10^{11}$ particles/ml) derived from genome-containing or genome-deficient particles of strain T3D were divided into aliquots of equivalent volume and incubated at either 4°C or over a range of temperatures (22-40°C) for 20 min. The reactions were chilled on ice and digested with 0.10 mg/ml trypsin for 30 min. Following addition of loading dye the samples were subjected to SDS-PAGE analysis. The position of major capsid proteins is shown. μ1 runs as μ1C.

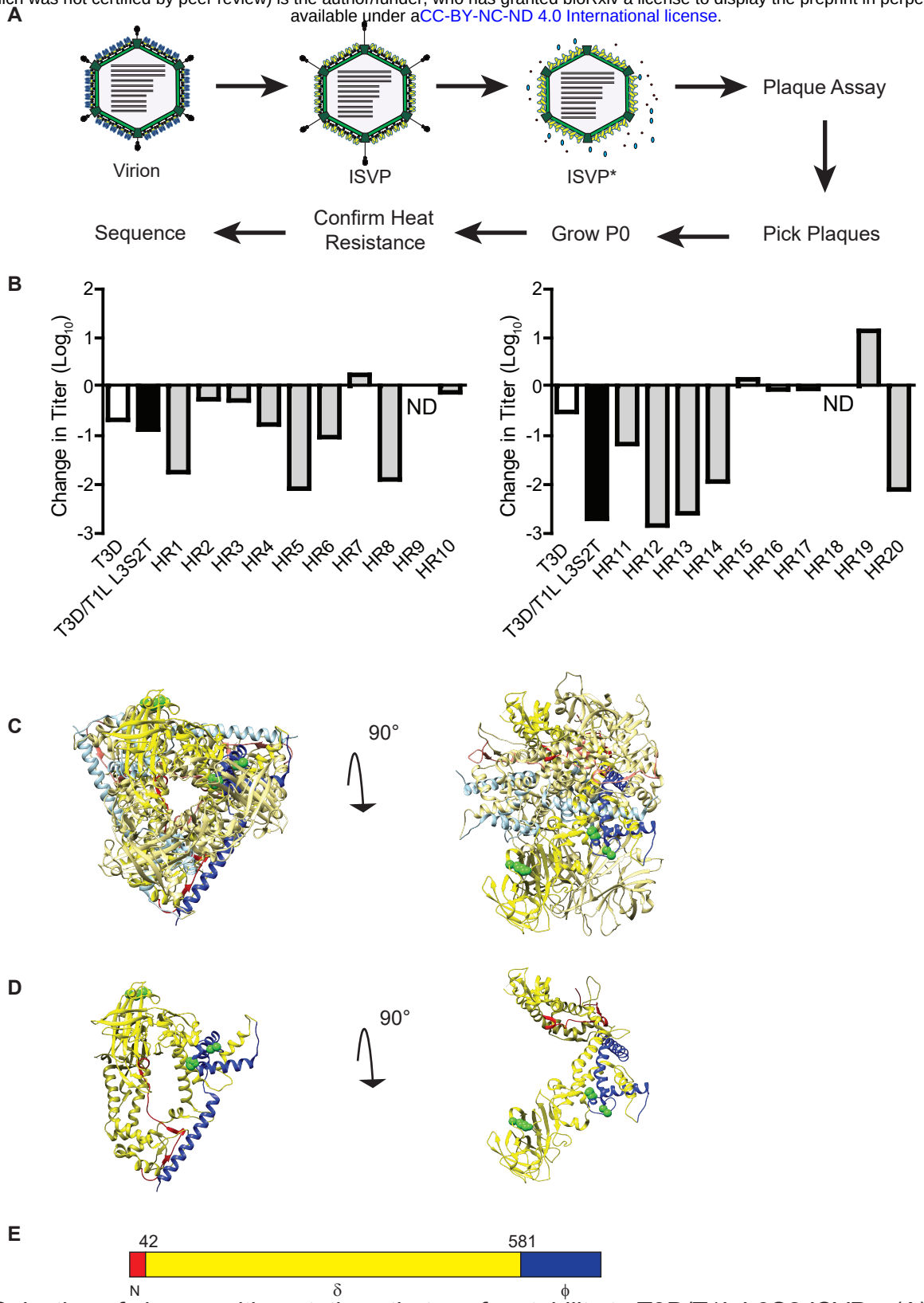

Figure 4. Selection of viruses with mutations that confer stability to T3D/T1L L3S2 ISVPs. (A) Diagram depicting the process for selecting for mutants with reduced ISVP-ISVP* conversion efficiency of T3D/T1L L3S2. ISVPs of T3D/T1L L3S2 were incubated at 40°C for 20 min. Reactions were then diluted in PBS and subjected to plaque assay. Viruses from resulting plaques were isolated and propagated to generate P0 stocks. Heat resistance of these putative heat resistant (HR) plaque isolates was confirmed by measuring the thermal stability of ISVPs incubated at 4°C or 40°C using a plaque assay. Mutants that were confirmed as heat resistant were sequenced. (B) ISVPs generated from P0 stocks were incubated at either 4°C or 40°C for 20 min. Reactions were then diluted in PBS and subjected to plaque assay. ND, Not detectable. (C, D) Top (left) and side (right) views of μ1 trimer (C) and monomer (D) are shown. Position of mutations identified in HR viruses are shown in green. μ1 cleavage fragments are colored as indicated (E) with one μ1 monomer shown with darker colors.

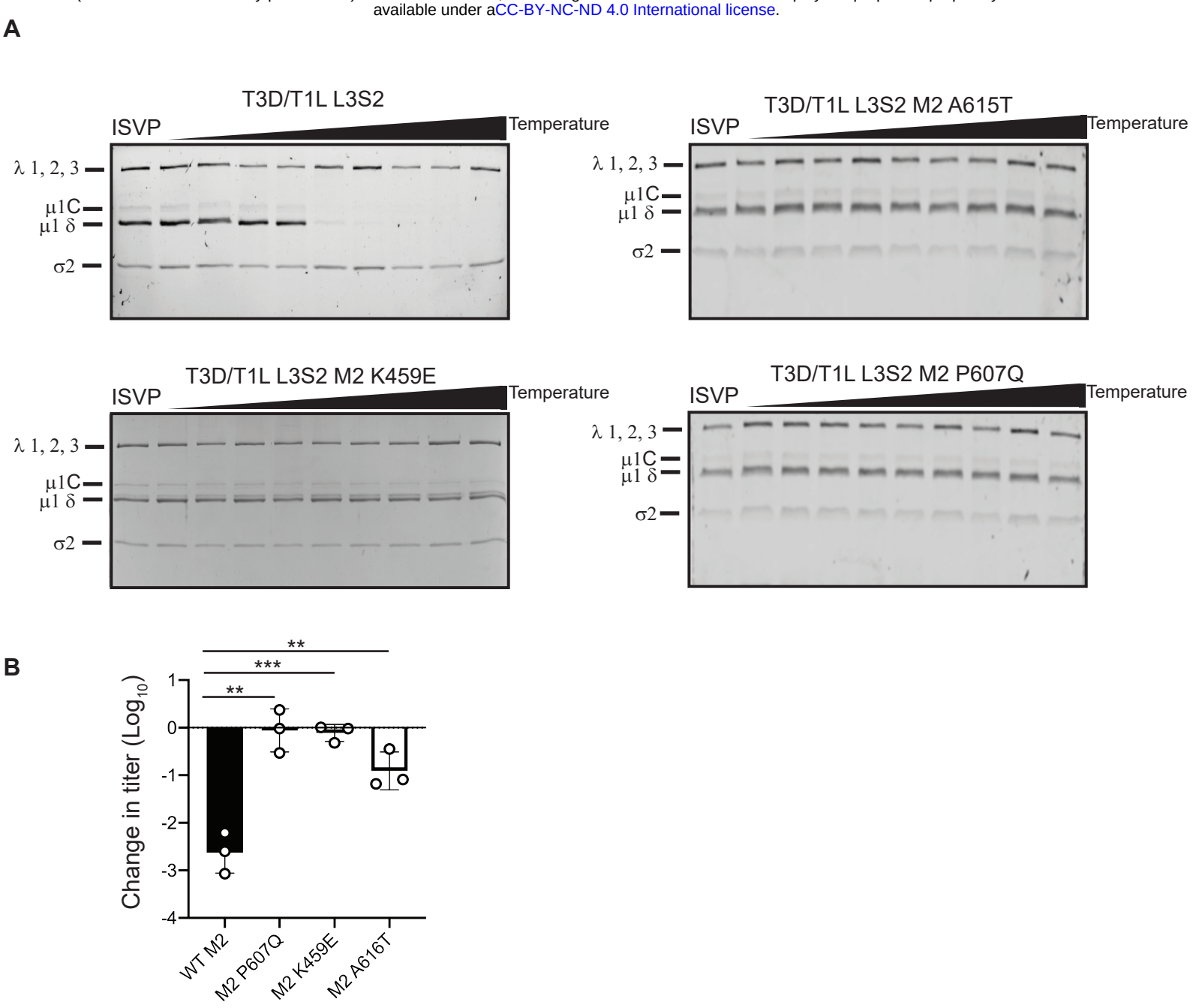

Figure 5. Mutations in μ1 restore stability of T3D/T1L L3S2. (A) ISVPs ($2x10^{11}$ particles/ml) of T3D/T1L L3S2 with the indicated M2 mutations were divided into aliquots of equivalent volume and incubated at either 4°C or over a range of temperatures (22-42°C) for 20 min. The reactions were chilled on ice and digested with 0.10 mg/ml trypsin for 30 min. Following addition of loading dye the samples were subjected to SDS-PAGE analysis. The gels shown are representative of at least 3 independent experiments. The position of major capsid proteins is shown. μ1 runs as μ1C. (B) ISVPs generated from P2 stocks of the indicated virus strain were divided into aliquots of equivalent volume and incubated at either 4°C or 40°C for 20 min. Reactions were then diluted in PBS and subjected to plaque assay. The data are plotted as mean loss of infectivity for three independent samples in comparison to samples incubated at 4°C. Error bars indicate SD. **, P<0.01, ***, P<0.001 as determined by student's t-test in comparison to T3D/T1L L3S2.

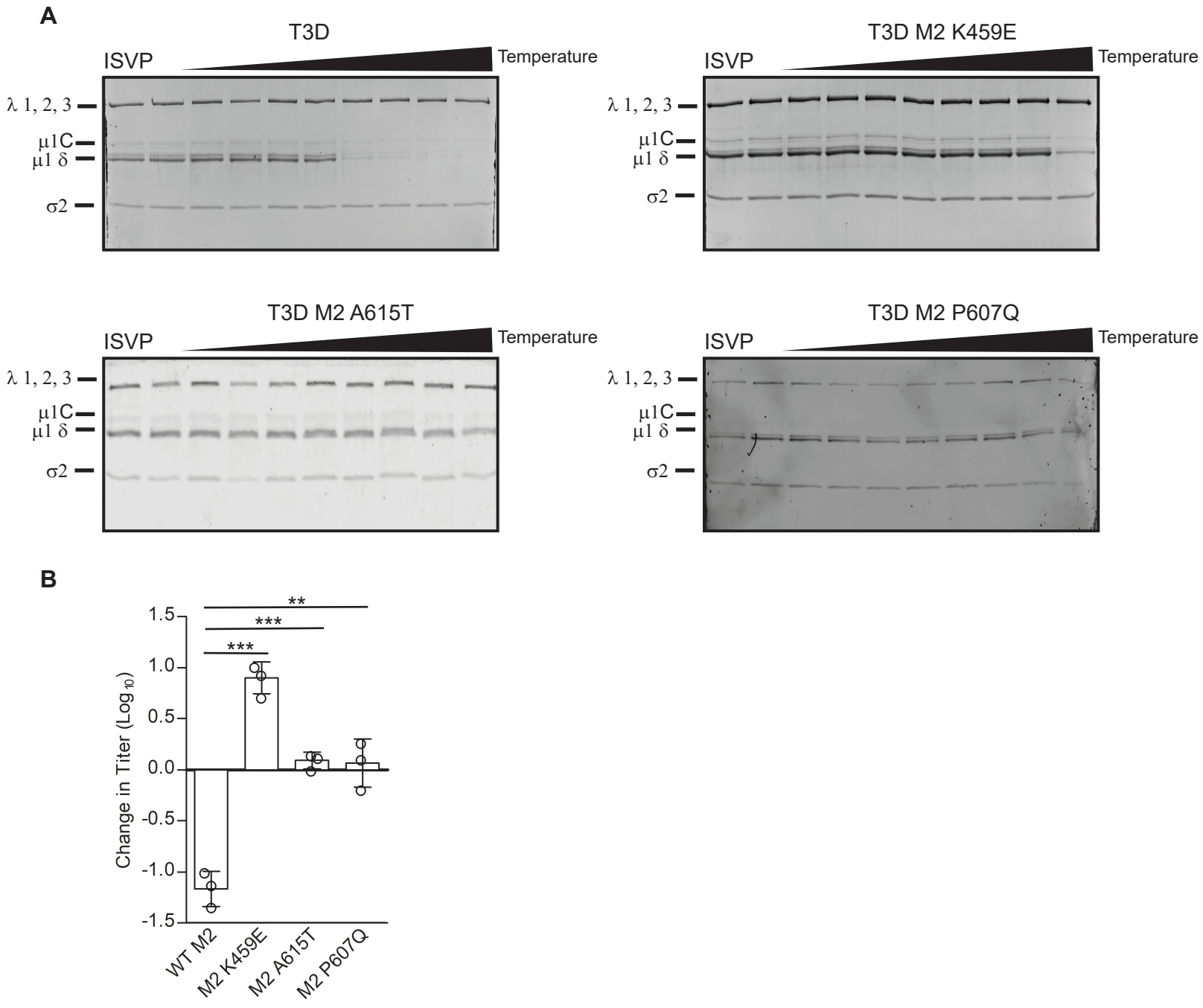

Figure 6. Mutations in μ1 hyperstabilize T3D. (A) ISVPs ($2x10^{11}$ particles/ml) of T3D and T3D with the indicated M2 mutations were divided into aliquots of equivalent volume and incubated at either 4°C or over a range of temperatures (32-46°C) for 20 min. The reactions were chilled on ice and digested with 0.10 mg/ml trypsin for 30 min. Following addition of loading dye the samples were subjected to SDS-PAGE analysis. The gels shown are representative of at least 3 independent experiments. The position of major capsid proteins is shown. μ1 runs as μ1C. (B) ISVPs generated from purified virions were divided into aliquots of equivalent volume and incubated at either 4°C or 42°C for 20 min. Reactions were then diluted in PBS and subjected to plaque assay. The data are plotted as mean loss of infectivity for three independent samples in comparison to samples incubated at 4°C. Error bars indicate SD. ***, P<0.001, **, P<0.01 as determined by student's t-test in comparison to T3D/T1L L3S2.

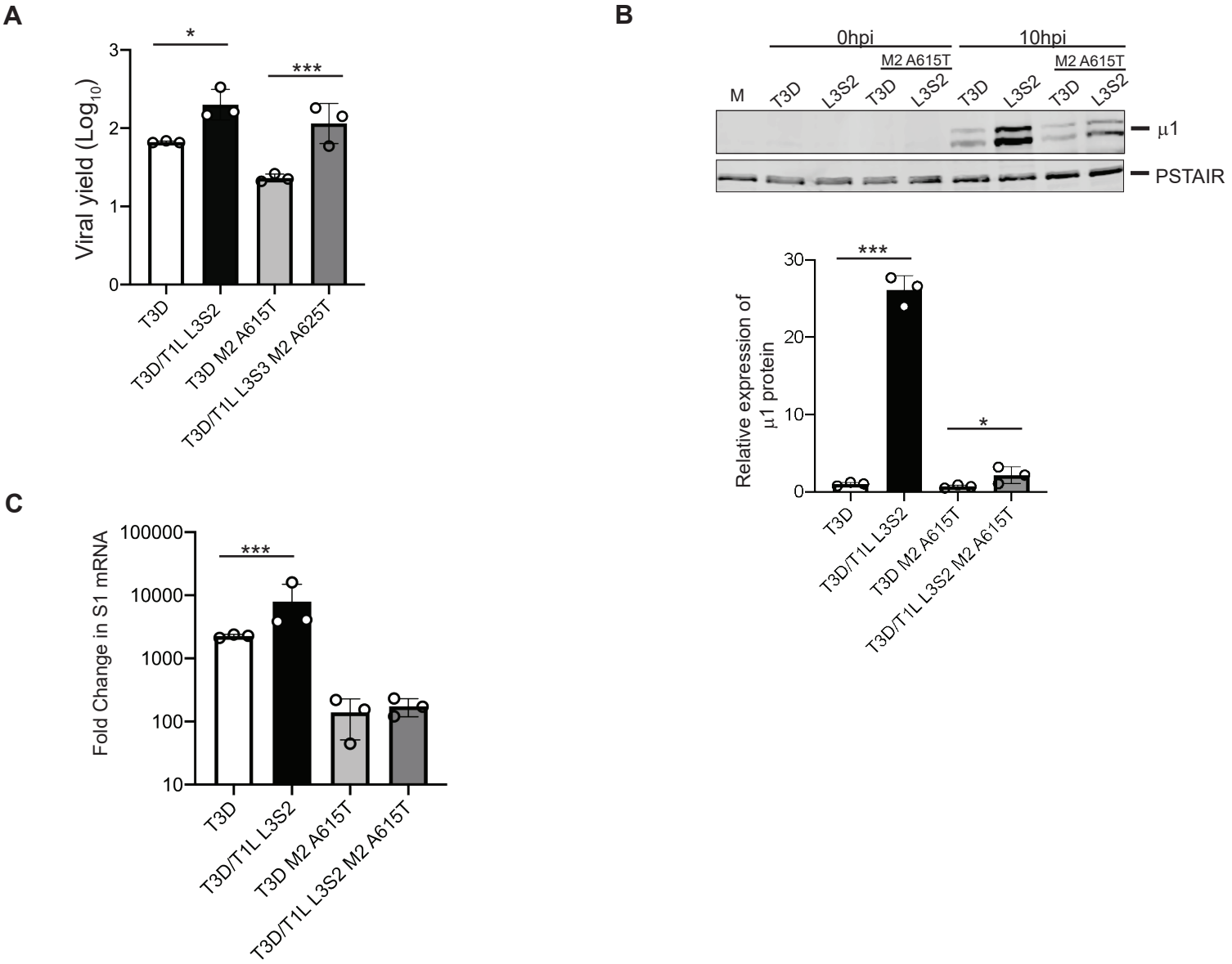

Figure 7. T3D/T1L L3S2 affects viral replication. (A) L cell monolayers were infected with T3D or T3D/T1L L3S2 or with the indicated mutant viruses at an MOI of 0.1 PFU/cell. At 0h and 24h post infection, the infected cells were lysed and the viral yield was quantified by plaque assay. Error bars indicate SD. *, P<0.05, ***, P<0.001 as determined by student's t-test in comparison to T3D. (B) L cell monolayers were infected with the indicated viruses at an MOI of 10 PFU/cell. At 10h post infection, the cells were lysed and protein production was determined by immunoblotting. Protein quantification of 3 replicates normalized to PSTAIR is shown. Error bars indicate SD. **, P<0.01, ***, P<0.001 as determined by student's t-test in comparison to T3D. (C) L cell monolayers were infected with the indicated viruses at an MOI of 10 PFU/cell. At the indicated times post infection, the cells were lysed and total RNA was isolated. cDNA was generated using primers for T3D S1 and GAPDH. mRNA production was measured by qPCR. Data shown are represented as fold change compared to mock infected samples and normalized to GAPDH. Error bars indicate SD. ***, P<0.001 as determined by student's t-test in comparison to T3D